A comparative study of scale-adaptive and large-eddy simulations of highly swirling turbulent flow through an abrupt expansion

Ardalan Javadi, Håkan Nilsson

Department of Applied Mechanics, Chalmers University of Technology, Gothenburg, SE-412 96, Sweden

E-mail: ardalan.javadi@chalmers.se

Abstract. The strongly swirling turbulent flow through an abrupt expansion is investigated using highly resolved LES and SAS, to shed more light on the stagnation region and the helical vortex breakdown. The vortex breakdown in an abrupt expansion resembles the so-called vortex rope occurring in hydro power draft tubes. It is known that the large-scale helical vortex structures can be captured by regular RANS turbulence models. However, the spurious suppression of the small-scale structures should be avoided using less diffusive methods. The present work compares LES and SAS results with the experimental measurement of Dellenback *et al.* (1988). The computations are conducted using a general non-orthogonal finite-volume method with a fully collocated storage available in the OpenFOAM-2.1.x CFD code. The dynamics of the flow is studied at two Reynolds numbers, $Re=6.0\times10^4$ and $Re=10^5$, at the almost constant high swirl numbers of $Sr=1.16$ and $Sr=1.23$, respectively. The time-averaged velocity and pressure fields and the root mean square of the velocity fluctuations, are captured and investigated qualitatively. The flow with the lower Reynolds number gives a much weaker outburst although the frequency of the structures seems to be constant for the plateau swirl number.

1. Introduction

If a confined jet is swirling sufficiently, a central stagnation point and a recirculation region is formed. A vortex breakdown usually occurs after the stagnation point due to the rapid expansion of a thin vortex into a much broader one [1]. Turbulent swirling flow through a sudden axisymmetric expansion possesses several distinctly different flow regimes, such as separation, one or two recirculation regions, high turbulence levels, and periodic asymmetries under some conditions. The vortex breakdown often triggers a large-scale precessing helical coherent structure. The diverging nature of the expansion flow is known to initiate and lock the location of the vortex breakdown and the flow instabilities. Many researchers have reported the experimental [2], analytical [3] and numerical investigations [4] of the vortex breakdown. This kind of flow is however still not well understood, especially for strongly swirling flow with swirl number about unity. The swirl number is defined as

$$Sr=\frac{1}{R}\frac{\int_0^R r^2 UW dr}{\int_0^R rU^2 dr} \quad (1)$$

where R is radios and r is radial position, W is axial and U is tangential velocity. There are only a handful detailed numerical studies which thoroughly analyze the coherent structures and vortex breakdown in sudden expansion [5-6]. The vortex breakdown occurs as the swirl number exceeds a critical value [7]. it is characterized by a wake-like velocity profile with a stagnation point, followed by flow reversal. At elevated swirl numbers ($Sr \geq 0.6$), the swirling jet emanating from the sudden expansion is deflected towards the wall, the outer recirculation region reduces and flow reversal becomes evident near the centerline of the expansion [8].

Swirling flow in sudden expansions has mostly been studied using conventional unsteady Reynolds-averaged Navier–Stokes (URANS) models [4]. Such models are primarily useful for capturing large-scale flow structures, while the details of the small-scale turbulence eddies are filtered out in the averaging process. To overcome this drawback, the scale-adaptive simulation technique (SAS) [9] is used in this study and the obtained results are compared with resolved large-eddy simulation (LES) results. The SAS model has an additional production term in the ω equation that increases when the flow equations start to go unsteady. The SAS term switches itself on when the ratio of the modelled turbulent length scale, $k^{1/2}/\omega$, to the von Karman length scale increases [10]. The von Karman length scale, is based on the ratio of the first to the second velocity gradients. The idea of the SAS term is that when the flow equations resolve unsteadiness, the SAS term detects the unsteadiness and increases the production of ω. The effect is that ω increases, and hence the turbulent viscosity decreases because ω appears in the denominator in the expression for ν_t and because the magnitude of the destruction term, in the modelled turbulent kinetic energy equation, increases. SAS models behave in many situations similar to Detached Eddy Simulation (DES) models [11-12], but without an explicit influence of the grid spacing on the RANS mode of the model [13]. The DES methods are also manipulated for industrial swirling flows by the authors. The authors ended up with better prediction of the on-axis recirculation region comparing RANS [18].

In this paper the k-ω SST SAS is evaluated and compared with a dynamic k-equation LES sub-grid scale model [15]. The strongly swirling flow through sudden expansion measured by Dellenback *et al.* [8] in studied for the operation conditions Re=6.0×10^4, Sr=1.16 and Re=10^5, Sr=1.23 which there is a strong on-axis recirculation region and helical vortex breakdown. The SAS method captures the main unsteadiness of the flow and shows good agreements with LES and experiment. The Reynolds number (Re) is defined as

$$Re = \frac{\rho W_b D}{\mu} \quad (2)$$

where W_b is bulk velocity, D is inlet radios, ρ is density and μ is dynamic viscosity.

2. Computational Framework

The governing equations are continuity and Navier-Stokes equations for incompressible flow. The equations are discretized using a general finite-volume method with a fully collocated storage, using the OpenFOAM-2.1.x CFD code. The CFD code is parallelized using domain decomposition and the Message Passing Interface (MPI) library. The simulations are performed using an AMD Opteron 6220 super computer and 128 cores. The second-order central difference scheme is used to discretize the diffusion terms, and the second-order linear upwind difference scheme is adopted to approximate the convection term. The time-marching is performed with an implicit second-order accurate backward scheme.

Regarding the presently investigated cases, with high Reynolds numbers and high level of turbulence anisotropy, turbulence models that do not assume a local balance between the energy production and dissipation rate have a much better potential for modeling the sub-grid stresses

correctly [15]. Backscatter of energy from the sub-grid scales to the resolved scales may occur if the sub-grid scales contain energy-containing eddies.

3. Computational Domain, Mesh Resolution and Boundary Conditions

The case studied in the present work is the swirling water flow through a sudden 1:2 axisymmetric expansion that was experimentally examined by Dellenback *et al.* [8]. The geometry and the experimental cross-sections are shown in Fig.1, the origin is located on centerline at expansion. Measurements of mean and RMS velocities were performed with a laser Doppler anemometer at several cross-sections, see Fig. 1a.

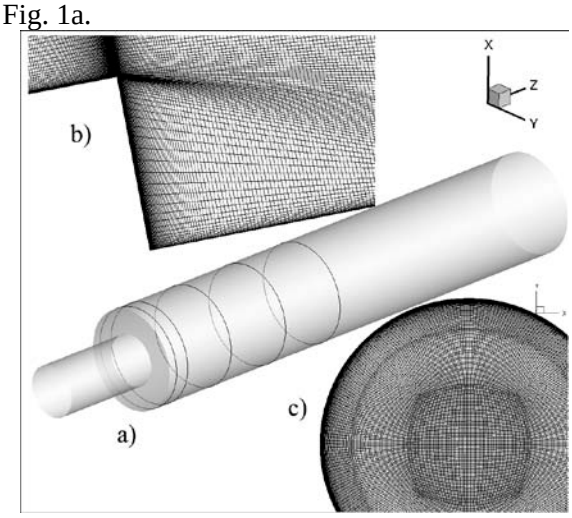

Figure1. Computational domain, a) experimental cross-sections, (z/D=0.25, 0.5,1 ,2 ,4) b) mesh configuration at expansion, c) mesh configuration at z/D=1.

The computational domain is extended 2D upstream of the expansion and 10D downstream of the expansion, to reduce the influence of the inlet and outlet boundary conditions. According to previous investigations, this domain raises least concerns about viable result [5-6]. The number of cells before and after the expansion is 1.35×10^6 and 6.61×10^6. The maximum CFL number in the entire the domain is in average 0.03, with a local maximum of 2. The inlet boundary condition for the mean velocity is constructed by spline curves based on the measured data. A boundary layer based on the log-law is added between the radially outermost measuring point and the wall as supported by Gyllenram *et al.* [4]. Earlier investigations of the same case by Schlüter *et al.* [17] showed that the turbulence level of the inlet boundary condition has large effects on the mean velocity profiles if the swirl level is low, while for high swirl flow the content of turbulence is less important due to high level of production in the flow field. Thus, the flow features are less independent of turbulence content at inlet. No slip condition is applied on the walls. After evaluation of outlet boundary conditions, homogenous Neumann condition, with restriction of the backflow for velocity and a homogenous Dirichlet condition for the pressure (z/D<2).

4. Result and discussion

The flow parameters are normalized with the inlet diameter D, and the inlet bulk velocity, W_b. Figure 2 shows the experimental and numerical mean axial and tangential velocity distributions of different turbulence treatments for the case with Re=10^5 and Sr=1.23. The numerical simulations are capable of capturing the main flow features with acceptable accuracy. For the axial velocity, both turbulence treatments predict a similar qualitative behavior of the on-axis recirculation region (r/D<0.5). It is worth mentioning that SAS presents a larger on-axis backflow especially in the downstream, see Fig. 2[c-f]. LES predicts higher tangential velocity than SAS in almost the entire domain. Figure 3 shows the experimental and numerical mean axial and tangential velocity distributions of the different turbulence treatments for the case with Re=6×10^4 and Sr=1.16.

There is a difference between consequent flow which tangential slot and vane generators produce. Tangential slot, the method which is used by Dellenback *et al.* [8], generates swirl flows produce a smaller, more compact recirculation bubble. Hence there are higher reverse velocities, higher gradients, higher turbulence intensities, and higher mixing rates associated with vortex breakdown bubbles produced by tangential inlets. In cases with the inlet swirl number of about unity, i.e. Sr=1.23 and 1.16 , the swirl reduces to Sr~0.4 right after the expansion and then increases to Sr~1.5 at z/D=1. Generally, this behavior can be related to the bubble type vortex breakdown which vanishes the axial and tangential velocity distribution over the cross section and gives higher swirl. Due to the vortex breakdown, the axial and tangential velocity vanish and appear in the same points, see Fig. 2 and 3, which leads to higher swirl number.

Figures 4 and 5 show the root mean square of the axial (w'_{rms}) and tangential (u'_{rms}) velocity fluctuations at different cross-sections. Since the swirl number is almost constant, the flow features are qualitatively similar and independent of Reynolds number. Due to the strong flow curvature after the expansion the SAS model, which is sensitive to velocity gradients, detects unsteadiness and resolve larger part of the flow. Thus, the SAS model predicts better than LES the turbulent structures after the expansion at this mesh resolution, see Figs. 4 and 5. The LES takes over the SAS in the downstream where the von Karman scale increases again and SAS models the flow.

Figure 6 shows the viscosity ratio of the flow at different cross-sections for both cases. The turbulent viscosity is calculated as

$$\upsilon_t = a_1 k / max(a_1\omega, SF_2) \quad , \quad F_2 = tanh(\eta^2) \, , \quad \eta = max\left(2k^{1/2}/\beta^* \omega d_w \, , \, 500\upsilon/d_w^2\omega\right) \qquad (3)$$

where a_1=0.31, $S=(2s_{ij}s_{ij})^{1/2}$, d_w is the wall distance, β^* =0.09. The interesting phenomenon in this flow field is that ω and the turbulent viscosity increase at the same time. This can be related to the high level of turbulence in the flow where the production of turbulent kinetic energy takes over the destruction of turbulent kinetic energy due to an increase in ω. Basically, when ω increases, the turbulent viscosity should decrease while Fig. 6 shows that turbulent viscosity increases at same distance after the expansion and then decreases. It is worth mentioning that there is a sudden decrease in turbulent viscosity for both cases on z/D=0.25 and at r/R=0.6. This can be related to the shear layer at separation edge which SAS model detects it very well. In the downstream where this free shear layer is less powerful, there no sense of decrease in the turbulent viscosity.

Figure 7 shows the intertwined and rich coherent structures of the flow. The vortex breakdown is clearly captured. The spiral form in particular reveals the suddenness of breakdown, and suggests the occurrence of a stagnation point at the vortex axis. The strength of vortices is in direct relation both with swirl and Reynolds numbers. The helical vortex before expansion and streaks are captured.

Figure 8 shows the power spectra density captured at (x/D, y/D, z/D)=(0, 0.5,0.25). The energy spectra show, that the dominant frequencies of the flow vary with the swirl number although the number and the magnitude of periodicities are independent of the Reynolds number. The power spectrum at the point shows that the flow is characterized by the existence of the vortex breakdown with dominant frequencies of about 0.75, 0.86, 1.47 and 1.71, respectively for Sr=1.23. The level of perturbation increases with the Reynolds number.

Conclusion

The Scale-adaptive simulation (SAS) based of SST k-ω model and a LES with a dynamic k-equation sub-grid model is used the swirling flow through a sudden expansion. Both models are capable of capturing the physics of the flow while SAS predicts better turbulent structures immediately after expansion. The case Re=6.0×10^4, Sr=1.16 has larger flow structures which LES presents better agreement comparing other operation condition, Re =10^5, Sr=1.23. The SAS model has an extra in ω equation which is responsible for detecting unsteadiness. The flow field after expansion is intertwined and unsteady. The SAS term switches itself on and increases the ω. This leads to increase the turbulent structures especially in the region after expansion.

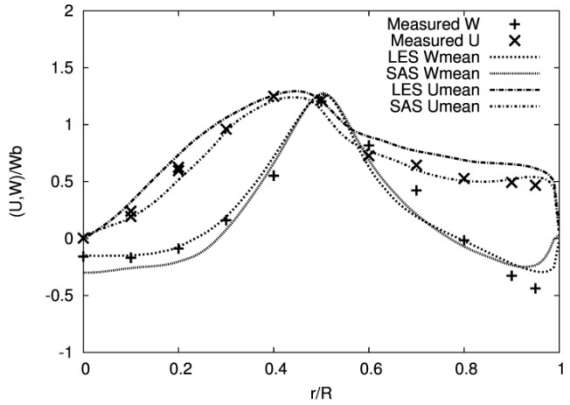

a) z/D=0.25

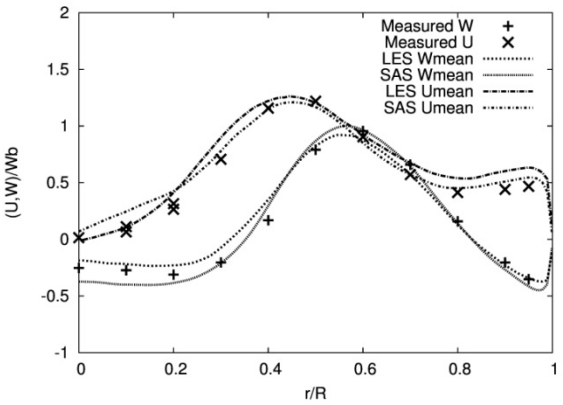

b) z/D=0.50

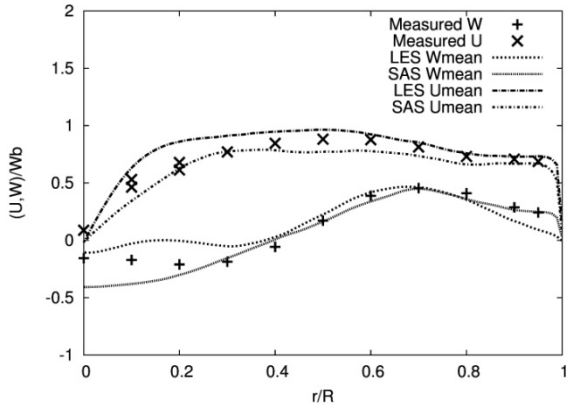

c) z/D=1.00

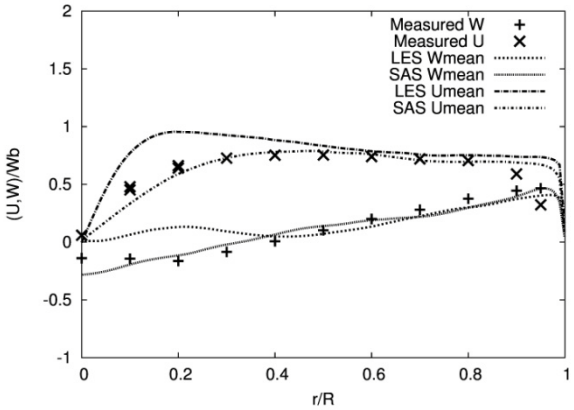

d) z/D=1.50

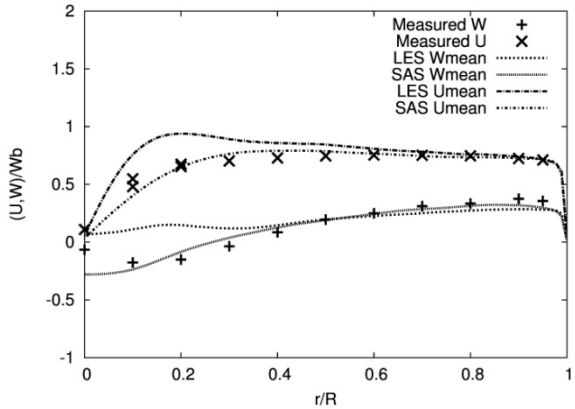

e) z/D=3.00

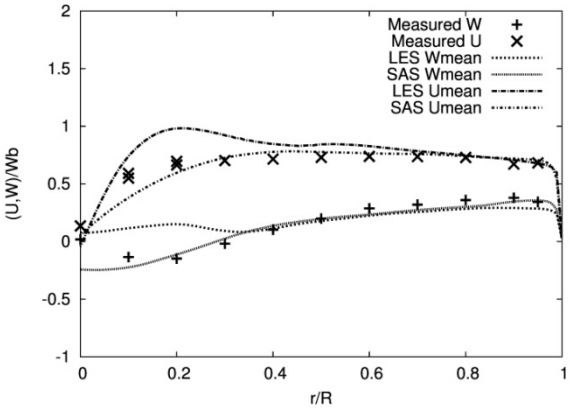

f) z/D=4.00

Figure 2. Axial, *W*, and tangential, *U*, velocity compared with experiment at different cross-sections for Re=10^5, Sr=1.23.

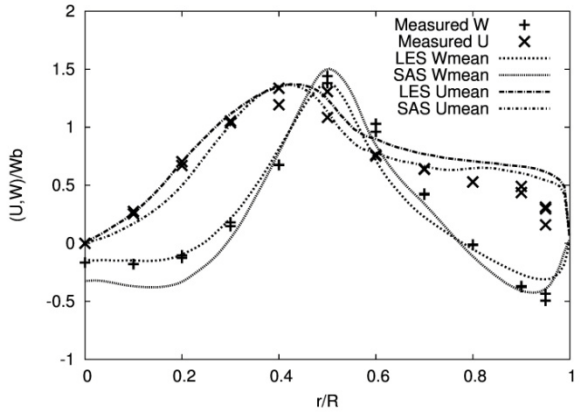

a) z/D=0.25

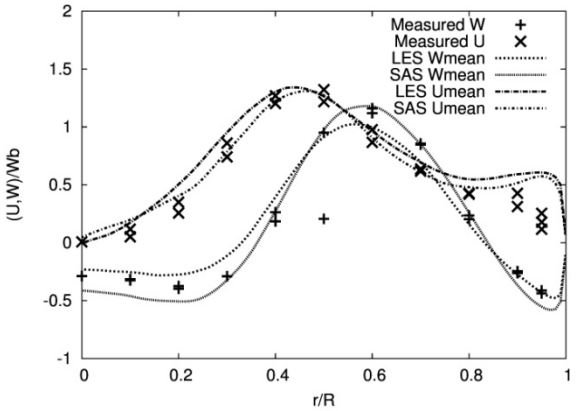

b) z/D=0.50

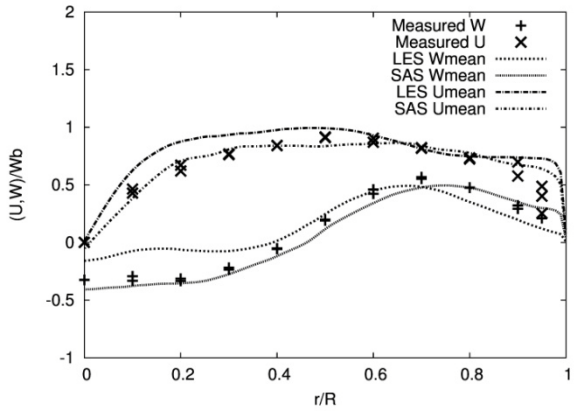

c) z/D=1.00

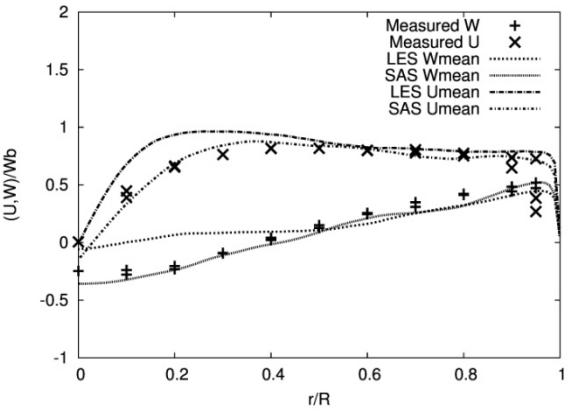

d) z/D=1.50

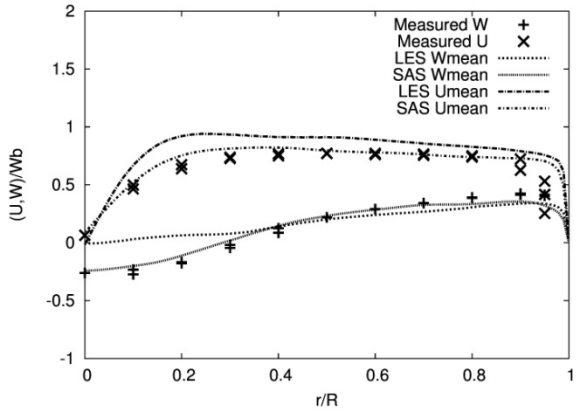

e) z/D=3.00

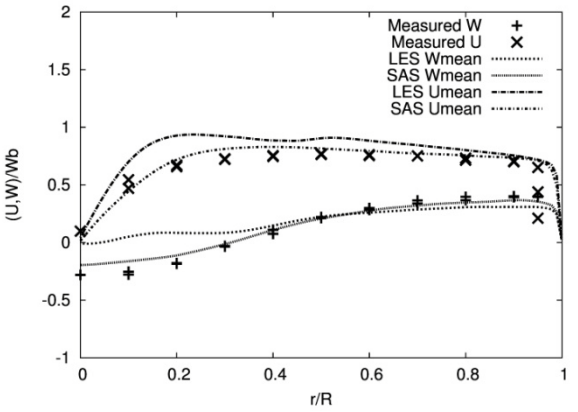

f) z/D=4.00

Figure 3. Axial, W, and tangential, U, velocity compared with experiment at different cross-sections for Re=6.0×10^4 , Sr=1.16.

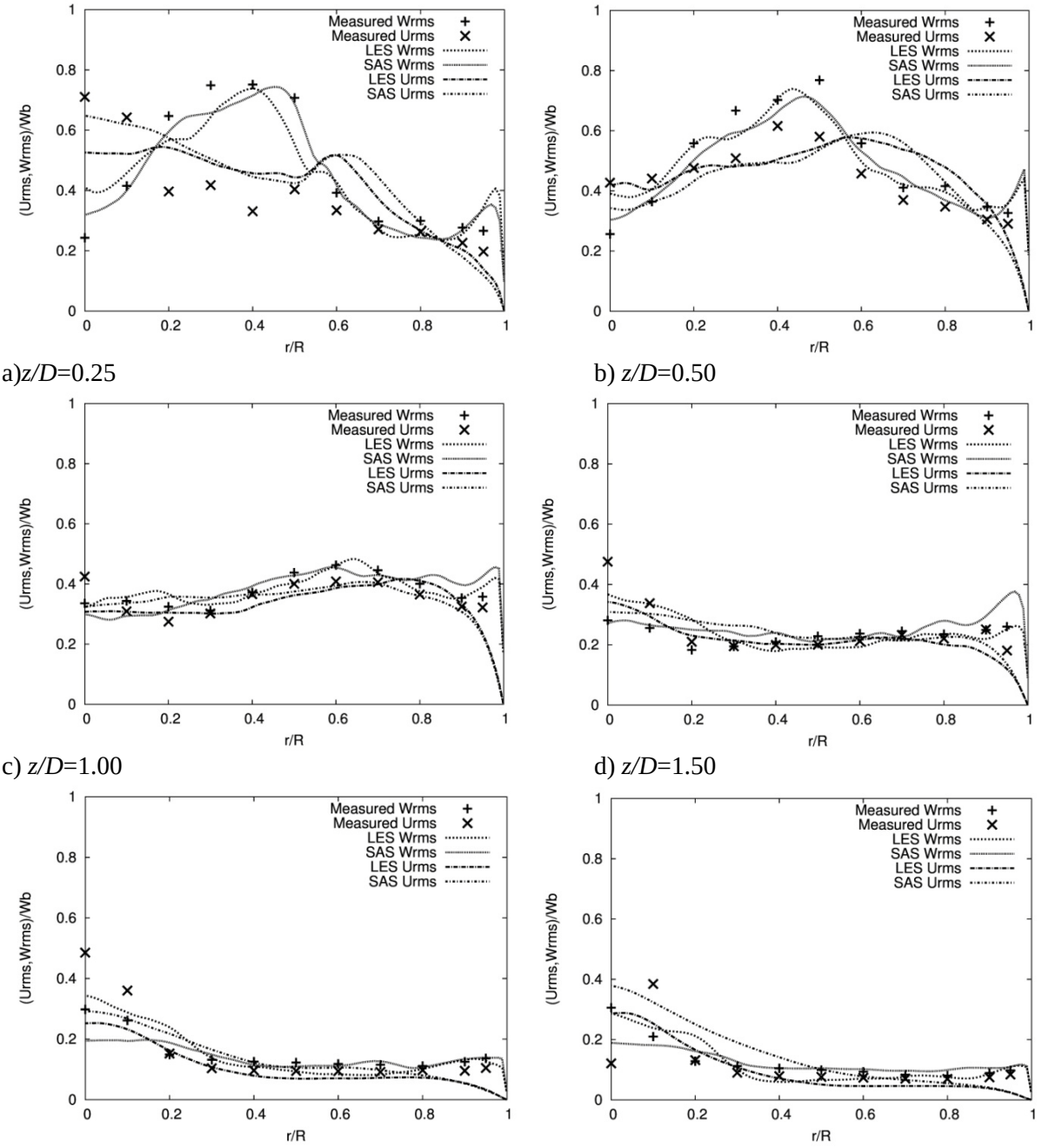

a)z/D=0.25 b) z/D=0.50

c) z/D=1.00 d) z/D=1.50

e) z/D=3.00 f) z/D=4.00

Figure 4. Axial, w'_{rms}, and tangential, u'_{rms}, velocity root mean square compared with experiment at different cross-sections for Re=10^5, Sr=1.23.

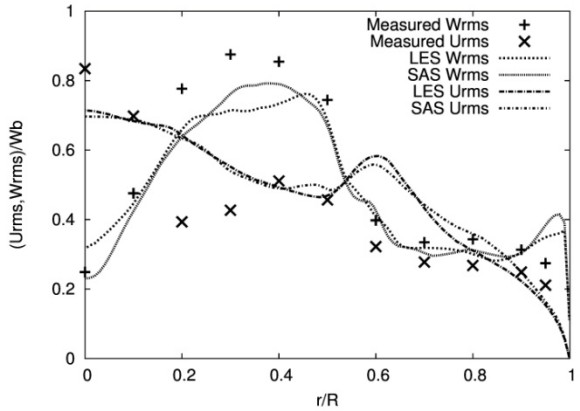

a) z/D=0.25

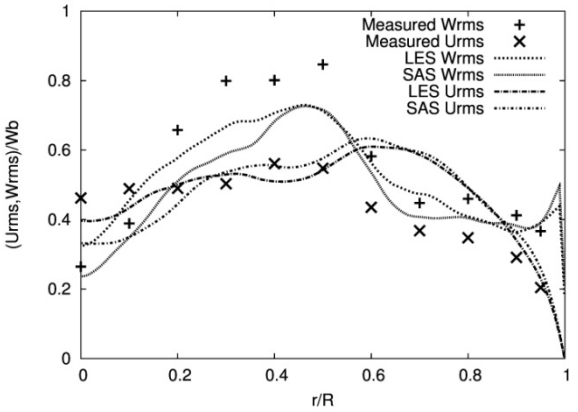

b) z/D=0.50

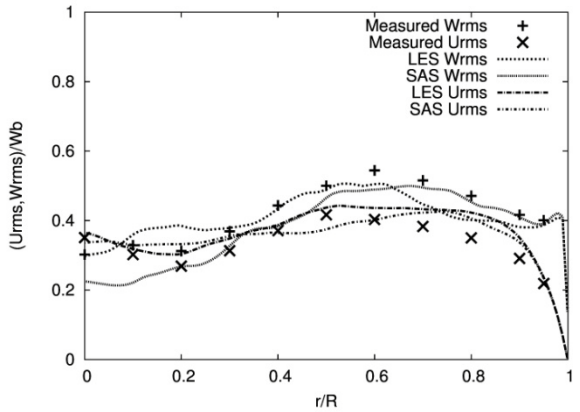

c) z/D=1.00

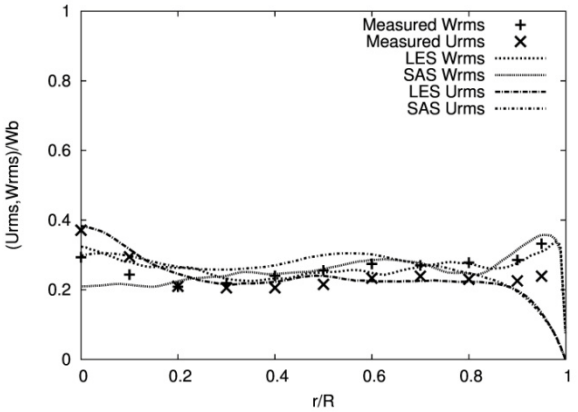

d) z/D=1.50

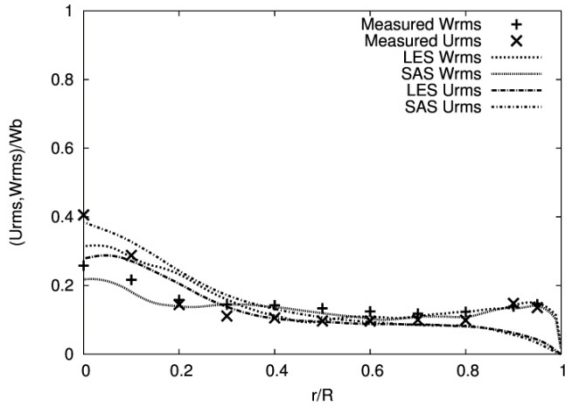

e) z/D=3.00

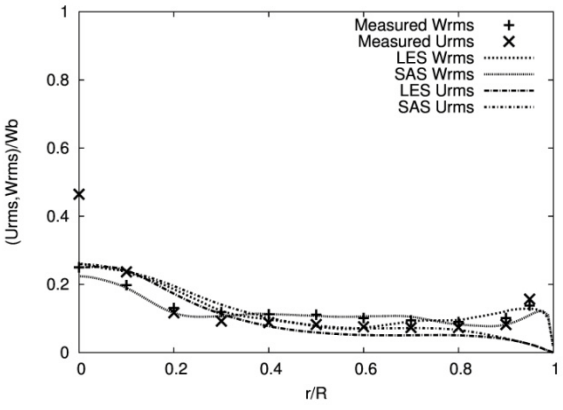

f) z/D=4.00

Figure 5. Axial, w'_{rms}, and tangential, u'_{rms}, velocity root mean square compared with experiment at different cross-sections for Re=6.0×10^4 Sr=1.16.

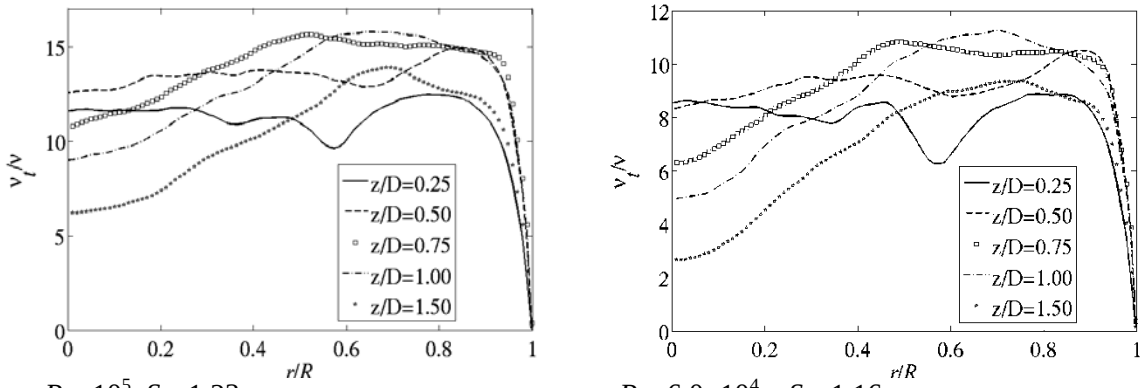

Re=10^5, *Sr*=1.23 *Re*=6.0×10^4 , *Sr*=1.16

Figure 6. Viscosity ratio of SAS for different cross-sections.

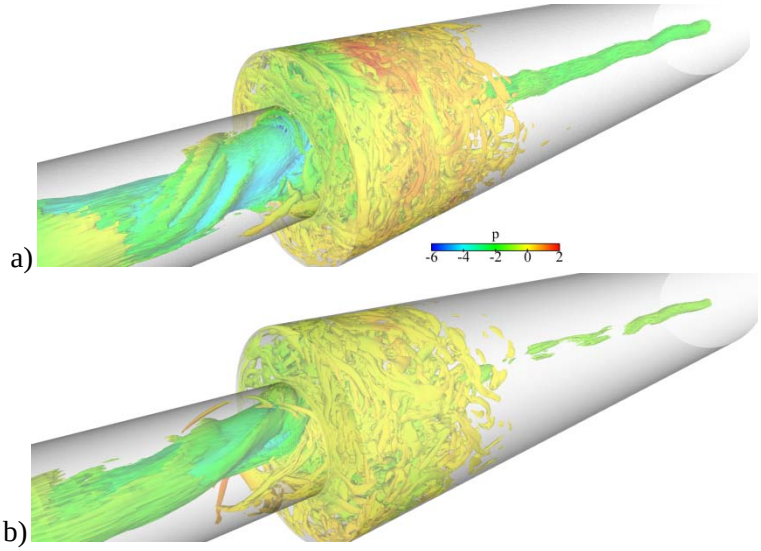

a)

b)

Figure 7. Vortex breakdown captured by LES visualized by instantaneous iso-surface of *q*-criterion colored by pressure for the case a) *Re*=10^5, *Sr*=1.23, b) *Re*=6.0×10^4 , *Sr*=1.16.

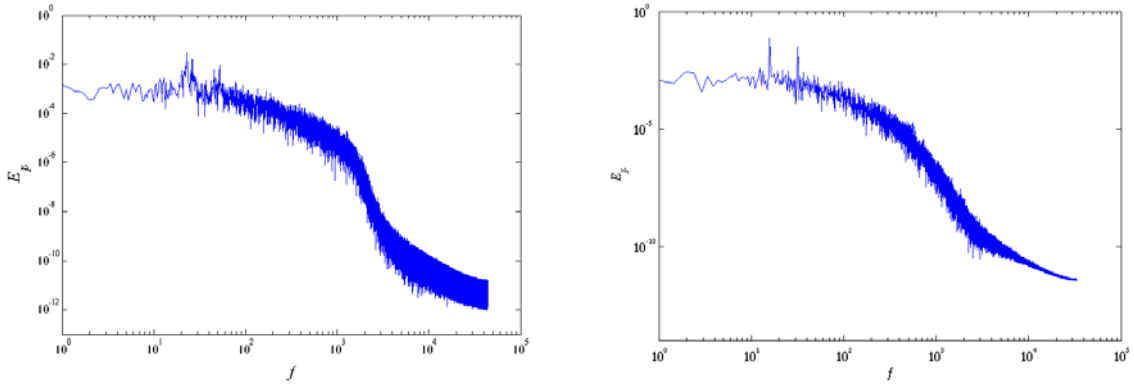

a) b)

Figure 8. Power spectra of velocity at (*x/D*, *y/D*, *z/D*)=(0, 0.5,0.25), for a) *Re*=10^5, *Sr*=1.23, b) *Re*=6.0×10^4 , *Sr*=1.16.

Acknowledgement
The research presented was carried out as a part of the ‘‘Swedish Hydropower Centre – SVC’’. SVC is established by the Swedish Energy Agency, Elforsk and Svenska Kraftnät together with Luleå University of Technology, The Royal Institute of Technology, Chalmers University of Technology and Uppsala University, www.svc.nu.

The computational facilities are provided by C^{3}SE, the center for scientific and technical computing at Chalmers University of Technology, and SNIC, the Swedish National Infrastructure for Computing.

References

[1] Leibovich S 1984 Vortex stability and breakdown: survey and extension *AIAA J,* **22**, 1192–1206
[2] Wang P, Bai X S, Wessman M and Klingmann J 2004 Large eddy simulation and experimental studies of a confined turbulent swirling flow, *Phys Fluids* , **16**, 3306. doi: 10.1063/1.1769420
[3] Gyllenram W, Nilsson H and Davidson L 2007 On the failure of the quasi-cylindrical approximation and the connection to vortex breakdown in turbulent swirling flow, *Phys Fluids*, **19**, 045108
[4] Nilsson H 2012 Simulations of the vortex in the Dellenback abrupt expansion, resembling a hydro turbine draft tube operating at part-load, *26th IAHR Symposium on Hydraulic Machinery and Systems*,(Beijing, China)
[5] Mak H and Balabani S 2007 Near field characteristics of swirling flow past a sudden expansion. *Chem Eng Sci* **62**, 6726–6746
[6] Gyllenram W, Nilsson H and Davidson L 2006 Large eddy simulation of turbulent swirling flow through a sudden expansion, *23rd IAHR Symposium on Hydraulic Machinery and Systems*, (Yokohama, Japan)
[7] Gyllenram W and Nilsson H 2008 Design and validation of a scale-adaptive filtering technique for LRN turbulence modeling of unsteady flow, *J. Fluid Eng.-T ASME*, **130**(5)
[8] Dellenback P A, Metzger D E and Neitzel G P 1988 Measurements in turbulent swirling flow through an abrupt axisymmetric expansion *AIAA J* **26**(6), 669–681
[9] Menter F R and Egorov Y 2005 A scale-adaptive simulation model using two-equation models *AIAA paper*, (Reno, NV)
[10] Davidson L 2006 Evaluation of the SST-SAS models: channel flow, asymmetric diffuser and axisymmetric hill, *European Conference on Computational Fluid Dynamics*, (Netherlands)
[11] Spalart P R 2009 Detached-eddy simulation, *Annu Rev Fluid Mech* **41**, 181–202
[12] Strelets M 2001 Detached Eddy simulation of massively separated flows, *AIAA Paper* 879
[13] Menter F R and Egorov Y 2010 The Scale-Adaptive Simulation method for unsteady turbulent flow predictions. Part 1: theory and model description, Flow, *Turbulence and Combustion*, **85** (1), 113-138
[14] Menter F R 1994 Two-equation eddy-viscosity turbulence models for engineering applications. *AIAA J* **32**(8), 1598–1605
[15] Kim W W and Menon S 1995 A new dynamic one-equation subgrid-scale model for large eddy simulations. *AIAA Paper*, (Reno, NV)
[16] Schlüter J U, Pitsch H and Moin P 2004 Large eddy simulation inflow conditions for coupling with Reynolds-averaged flow solvers *AIAA J* **42** (3), 478–484
[17] Javadi A and Nilsson H 2014 LES and DES of swirling flow with rotor-stator interaction, *5th symposium of hybrid RANS-LES method*, (Texas A&M university, USA)